Journal of Materials Chemistry C

Facile p-n Control, Magnetic and Thermoelectric Properties of Chromium Selenides Cr2+xSe3

Journal:	*Journal of Materials Chemistry C*
Manuscript ID	TC-ART-03-2019-001634.R3
Article Type:	Paper
Date Submitted by the Author:	29-May-2019
Complete List of Authors:	Guo, Quansheng; National Institute for Materials Science, Thermal Energy Materials Group Berthebaud, David; CNRS-Saint Gobain-NIMS, UMI 3629, Laboratory for Innovative Key Materials and Structures (LINK) Ueda, Jumpei; Kyoto University, Tanabe, Setsuhisa; kyoto university, Grad School of HES; Kyoto University Miyoshi, Akinobu; Tokyo Institute of Technology, Chemitry Maeda, Kazuhiko ; Tokyo Institute of Technology, Chemistry Mori, Takao; National Institute for Materials Science,

Journal of Materials Chemistry C - TC-ART-03-2019-001634 Revised Version

Facile p-n Control, Magnetic and Thermoelectric Properties of Chromium Selenides $Cr_{2+x}Se_3$

Quansheng Guo, [†] David Berthebaud, [₸] Jumpei Ueda, [§] Setsuhisa Tanabe, [§] Akinobu Miyoshi, [ǀ] Kazuhiko Maeda, [ǀ] and Takao Mori [†‡*]

[†] Center for Functional Sensor & Actuator (CFSN) & WPI Center for Materials Nanoarchitechtonics (WPI-MANA), National Institute for Materials Science (NIMS), Namiki 1-1, Tsukuba 305-0044, Japan

[₸] CNRS-Saint Gobain-NIMS, UMI 3629, Laboratory for Innovative Key Materials and Structures (LINK), National Institute for Materials Science, Tsukuba 305-0044, Japan

[§] Graduate School of Human and Environmental Studies, Kyoto University, Kyoto 606-8501, Japan

[ǀ] Department of Chemistry, School of Science, Tokyo Institute of Technology, 2-12-1-NE-2 Ookayama, Meguro-ku, Tokyo 152-8550, Japan

[‡] Graduate School of Pure and Applied Sciences, University of Tsukuba, Tennoudai 1-1-1, Tsukuba 305-8671, Japan

Corresponding author: MORI.Takao@nims.go.jp

ABSTRACT

Cr_2Se_3 crystallizes in a NiAs-type structure and is antiferromagnetic with a Néel temperature T_N = 43 K (M. Yuzuri, 1973). Here seven samples with the nominal composition $Cr_{2+x}Se_3$ (x = –0.04, –0.02, 0, 0.04, 0.06, 0.08 and 0.12) were prepared by solid state reaction and spark plasma sintering (SPS). The phase composition was characterised by X-ray diffraction (XRD). All compounds were studied through electrical conductivity, Seebeck coefficient, thermal conductivity, and Hall effect measurements. Both Seebeck coefficients and Hall coefficients show that $Cr_{2+x}Se_3$ are *p*-type materials when x = –0.04, –0.02, 0 and 0.04, and switch to *n*-type when x = 0.06, 0.08 and 0.12. An effective magnetic moment μ_{eff} = 3.85 μ_B per Cr ion in Cr_2Se_3 is obtained by Curie-Weiss law. We also calculate and compare band gap values of $Cr_{2+x}Se_3$ acquired through various methods, such as Arrhenius formula, Goldsmid-Sharp equation and optical spectrum. Moderate zT values are obtained for *p*-type $Cr_{2.04}Se_3$ and *n*-type $Cr_{2.08}Se_3$ at relatively low temperature above room temperature. These results exemplify the availability of *p*- and *n*- type legs from binary transition metal chalcogenides and reveal their potential for wide scale thermoelectric applications.

INTRODUCTION

Thermoelectric power generators are composed of *n*-type and *p*-type thermoelectric couples that are connected electrically in series and thermally in parallel, and are capable of converting waste heat from combustion of fossil fuel, for example, directly into electricity.[1] There is also a large need to develop energy harvesting technologies to power IoT (Internet of Things) sensors and devices.[2, 3] Thermoelectrics is considered promising since it can utilize body heat and small temperature differences in the environment to power ubiquitous sensors.[4, 5] The efficiency (η) of thermoelectric power generation technology can be expressed as

$$\eta = \frac{T_H - T_C}{T_H} \frac{\sqrt{1+zT}-1}{\sqrt{1+zT}+T_C/T_H}$$

with T_H = hot side temperature, T_C = cold side temperature. η is a parameter determined by the materials' dimensionless figure-of-merit, $zT = \sigma\alpha^2 T/\kappa$, where σ, α, κ and T refer to the electrical conductivity, Seebeck coefficient, thermal conductivity and the absolute temperature, respectively.[6, 7] Obtaining high zT is challenging, because σ, α, κ are all closely related to the charge carrier concentration and difficult to be independently optimized. In general, a carrier concentration 10^{19} to 10^{21} cm^{-3} is assumed to be required to fabricate advanced thermoelectric materials.[8]

In the past several decades, worldwide intensive efforts have accelerated the development of high performance thermoelectric materials. Many *p*-type materials have been discovered, including $Bi_{0.5}Sb_{1.5}Te_3$ enhanced via stable nanostructuring, zT

= 1.22 at 340 K,[9] via stable energy filtering, zT = 1.51 at 350 K,[10] PbTe–4mol%SrTe–2%Na with zT = 2.2 at 915 K,[11] and $Yb_{14}Al_{0.8}Mn_{0.2}Sb_{11}$ with zT = 1.3 at 1223 K.[12] In the meanwhile, a vast number of promising *n*-type materials are also established, such as skutterudites $Sr_{0.09}Ba_{0.11}Yb_{0.05}Co_4Sb_{12}$ and $CoSb_{2.75}Si_{0.075}Te_{0.175}$ with zT = 1.6 ~ 1.9 at around 800 K,[13, 14] Sb\Bi-doped Mg_2Si-Mg_2Sn solid solutions with zT = 1.3 ~1.4 at 700 K,[15, 16] the Zintl phase $Mg_{3.2}Sb_{1.5}Bi_{0.49}Te_{0.01}$ with zT = 1.51 at 716 K,[17] *etc*. There is also a recent interest to investigate magnetic compounds, like magnetic transition element chalcogenides that have exhibited high power factors − Cr_2S_3, [18, 19] $CuFeS_2$, [20-22] $CuCr_2S_4$, [23] and $Cu_4Mn_2Te_4$. [24] The thermoelectric properties of antiferromagnetic rhombohedral Cr_2Se_3 with the space group $R\bar{3}$,[25] have also been intensively studied. Although magnetic properties were not studied, transition metals (Mn, Ni, Nb and Ag) doping on the Cr site resulted in an increase of ~25% in zT.[26, 27] The revisit to the Cr_2S_3-Cr_2Se_3 which was first studied in the 1970s,[28] also emphasises the importance of exploring magnetic transition metal chalcogenides as attractive thermoelectric materials.[29]

Magnetic ion doping into nonmagnetic chalcogenides has also led to enhancement of power factors in cases where strong correlation between the magnetic ion and carriers were realised, leading to enhanced effective mass.[30-32] Spin fluctuation has also recently been demonstrated as an enhancer of power factor.[33]

To our knowledge, there are comparatively few reports on superior cost-efficient and environmentally friendly thermoelectrics with both *n*- and *p*-type in the same materials system. When it comes to module construction and application, both *n*- and

p-type legs made of the same material system are ideal candidates in terms of similar chemical and physical parameters like melting points and thermal expansion coefficients.[34] Previously in our group it was demonstrated that excellent *n*-type and *p*-type borides could be obtained in the $Y_{0.57}Al_yB_{14}$ system by varying the fractional occupancy of Al.[35] High Seebeck coefficients α = 400 μV K^{-1} was found for *p*-type sample with y = 0.41 and α = –200 μV K^{-1} for *n*-type sample y = 0.62, which means $Y_{0.57}Al_yB_{14}$ system is promising for high temperature thermoelectric power generation. Zr doping into elemental boron also yielded large p-type and n-type Seebeck coefficients.[36] Inspired by our work on the $Y_{0.57}Al_yB_{14}$ system where variation of the Al occupancy led to p-n control, and focusing on the previous reported *p*-type ternary or quaternary modifications of Cr_2Se_3,[26-29] we developed both *n*- and *p*- type binary chromium selenides $Cr_{2+x}Se_3$ aiming for applications near room temperature by atomic ratio manipulation in this contribution. And we also revealed the dependence of magnetic, electrical and thermal properties on stoichiometry.

EXPERIMENTAL PROCEDURES

Synthesis and Phase Purity Analysis. Samples with nominal composition $Cr_{2+x}Se_3$ (x = –0.04, –0.02, 0, 0.04, 0.06, 0.08, and 0.12) were prepared directly from high purity elements chromium chips (99.995%, Sigma Aldrich) and selenium powder (99.99%, –100 mesh, Sigma Aldrich). The elements were weighed according to the chemical formulae Cr : Se = (2+x) : 3, mixed in an agate mortar, transferred into

carbon-coated silica tubes and sealed under vacuum by an oxygen-acetylene torch. The ampoules were put vertically into a programmable resistance box furnace, heated to 1273 K at a slow rate of 10 K/h, held for 24 hours and eventually quenched to room temperature in a water bath. The phase compositions were characterized by powder X-ray diffraction (XRD, SmartLab3, Rigaku) with Cu $K\alpha$ radiation.

Consolidation. After quenching, the samples were ground into powder in an agate mortar by hand. Then the powder was loaded into a graphite die with a diameter of 10 mm and sintered by spark plasma sintering (SPS, SPS-1080 System, SPS SYNTEX INC). The SPS sintering temperature, sintering time and sintering pressure are 923 K, 5 min and 60 MPa, respectively. The sintering was performed in an argon atmosphere under a pressure of about 0.09 MPa.

Physical Properties Measurement. The thermal diffusivity λ was measured with the laser flash method (TC7000, Ulvac Thermal Analysis) under dynamic vacuum from 350 K up to 800 K. At each temperature point, three measurements were conducted and the averaged results are presented herein. The density d was calculated according to the ratio of mass to volume, which yielded 95 - 99% of the theoretical values (Table 1). The specific heat capacity C_p was estimated following the Dulong-Petit law. The thermal conductivity κ was then calculated using the formula $\kappa = \lambda C_p d$, which roughly has an experimental error of $\pm 5\%$.

After thermal diffusivity measurement, rectangular bars were cut out of the disks for electrical properties measurement. The electrical conductivity and Seebeck coefficient values were obtained simultaneously on a commercial instrument (ZEM-2, Ulvac-Riko). The measurement was carried out under a standard four-probe configuration and a helium atmosphere. The experimental uncertainty in electrical conductivity and Seebeck coefficient are estimated to be around $\pm 7\%$ and $\pm 5\%$, respectively. No obvious temperature hysteresis in thermoelectric properties upon cycling was observed (Figure S1). For the sake of clarity, only one of *n*-type sample $Cr_{2.08}Se_3$ with the best general performance will be discussed in the following sections.)

Room temperature Hall effect for $Cr_{2+x}Se_3$ (x = –0.04, –0.02, 0, 0.04, 0.08) was measured on the Physical Properties Measurement System (PPMS, Quantum Design) with the AC transport option. The data was taken with magnetic field sweeping from –5 T to +5 T. The carrier concentration n was calculated from $n = 1/eR_H$ (R_H = Hall coefficient) and carrier mobility μ calculated from $\mu = 1/ne\rho$ (ρ = electrical resistivity).

Microstructure Characterization. The microstructure and elemental distribution of $Cr_{2+x}Se_3$ (x = –0.04, 0, 0.08) were characterized by field emission scanning electron microscopy (FESEM, Hitachi S-4800) equipped with an energy dispersive spectrometer (EDS, Horiba EMAXEvolution X-Max). The elemental ratios for

samples with x = –0.04, 0, 0.08 were determined as Cr : Se = 39.2: 60.8, 38.0 : 62.0 and 39.3 : 60.7 at.%, respectively. Each result compares reasonably well with the nominal composition.

Optical Measurement. UV-Visible-Near Infrared diffuse reflectance spectra (UV-Vis-NIR DRS) of $Cr_{2+x}Se_3$ (x = –0.04, 0, 0.08) were also measured by JASCO V-670 spectrophotometer in the wavelength range of 200 nm – 2700 nm. Diffuse reflectance spectrum of a pellet of Cr_2Se_3 was measured by a spectrophotometer (Shimadzu, UV-3600) and its band gap was estimated from the Tauc plot under the condition of direct allowed transition.[37] Both measurements yielded $E_g(Cr_2Se_3)$ = 0.4 ~ 0.46 eV, which is in good agreement with the energy of absorption edge (0.3 eV) obtained from the reflectance spectrum in the previous paper.[38]

Magnetic Properties Measurement. The magnetization M was measured on $Cr_{2+x}Se_3$ (x = –0.04, 0, 0.08) at a constant external field H = 100 Oe in the temperature range of 4 – 300 K using the Magnetic Properties Measurement System (MPMS, Quantum Design). A small piece of sample weighted ~20 mg was loaded into a gelatine capsule for the measurement. The magnetic susceptibilities (χ) were calculated as the ratio of M/H. Therefore the molar susceptibility (χ_M) was determined.

RESULTS AND DISCUSSIONS

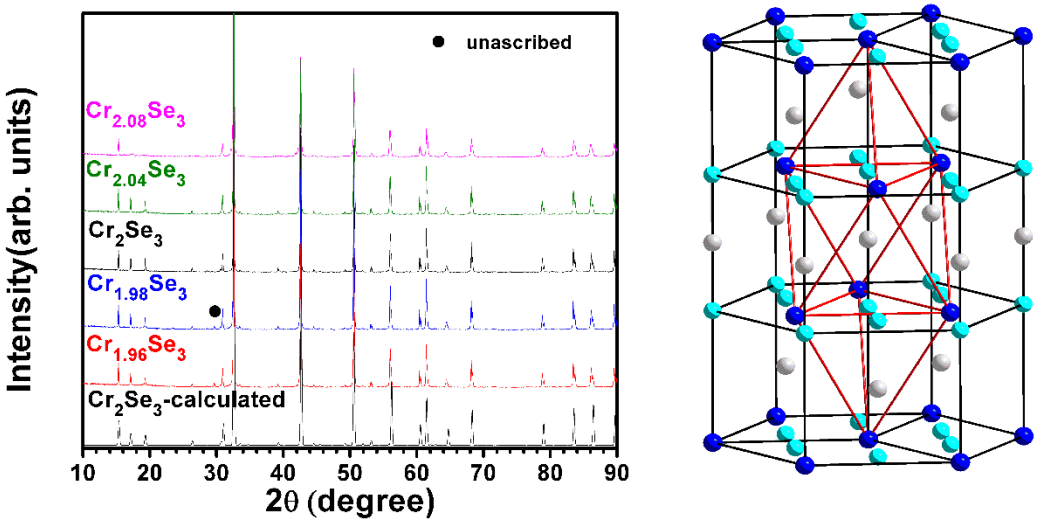

Figure 1. Left: Powder XRD patterns for $Cr_{2+x}Se_3$ at room temperature. Right: Crystal structure of rhombohedral Cr_2Se_3 shown in hexagonal mode. The red lines describe a rhombohedral unit cell. Blue: Cr at *3a* site; Grey: Cr at *3b* site and Cyan: Cr at *6c* site. The Se atoms are not shown for the sake of clarity.

The phase compositions were performed *via* powder X-ray diffraction using SmartLab3 with Cu *K*α radiation. The powder XRD patterns are shown in Figure 1(left). In each case the main phase could be indexed to the rhombohedral Cr_2Se_3, the crystal structure of which is shown in Figure 1(right). In Cr_2Se_3, two thirds of the octahedral sites in alternate cation layers are vacant, forming the layer sequence $A\gamma B$ $\gamma_{1/3}A\gamma B\gamma'_{1/3}A\gamma B\gamma''_{1/3}$ (A and B denote the postitions of layers of Se atoms; γ = octahedral interstices). As also observed from Figure 1(left), a tiny unascribed peak was found in samples with x = –0.04 and x = –0.02. For the sample with x = 0.08, symmetry is changing from $R\bar{3}H$ to $P3m1$, characterised by the decreased diffractions at 15~20°, while the framework remains the same as $P3m1$ structure is

a reduced average cell from $R\bar{3}H$. No obvious peak shift was observed at higher angles. The Rietveld refinements of $Cr_{2+x}Se_3$ (x = –0.04, 0, 0.08) using the GSAS program[39] via the graphical interface EXPGUI[40] reveal the slight changes in the lattice parameters (Table S1).

Pellets of the samples with x = –0.04, 0 and 0.08 after SPS procedure were analyzed by energy dispersive spectroscopy (EDS) using an acceleration voltage of 15 kV. No other impurity elements were detected in our samples within the detection limit. It appeared that the distributions of the elements are homogeneous on the micron scale (Figure 2).

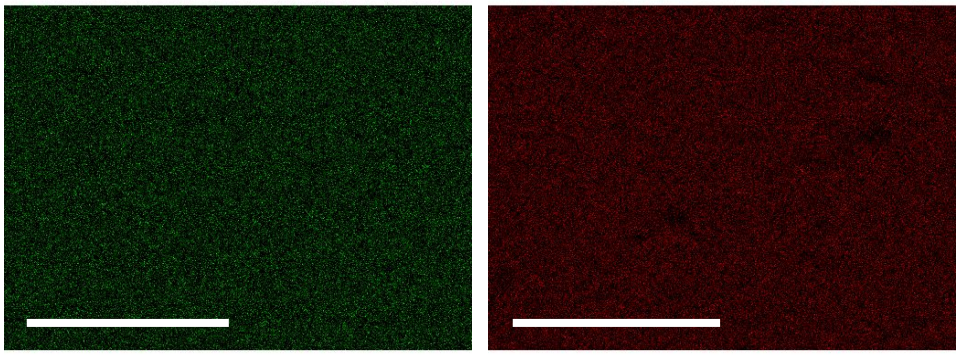

Figure 2. EDS mapping results of Cr_2Se_3. Left : Cr and right: Se. The horizontal bars define a length of 30 μm.

Temperature–dependent direct current magnetization was first measured from 5 K to 300 K to get zero-filed-cooled (ZFC) magnetization, and then back to 5 K as the field cooled (FC) magnetization. Figure 3 shows the zero field cooled (ZFC) and field cooled (FC) magnetic susceptibilities χ of $Cr_{2+x}Se_3$ (x = –0.04, 0 and 0.08). As the temperature increases, the molar magnetic susceptibility χ_M begins to increase

drastically at around 30 K because of a transition from low temperature antiferromagnetic AFM(L) phase to high temperature antiferromagnetic phase AFM(H),[41] and then arrive at the maximum at 50 K, which is consistent with the results by Adachi *et al.*[42] *M* is irreversible for field-cooling (FC) and zero-field-cooling (ZFC) in the cases of pristine Cr_2Se_3 and $Cr_{2.08}Se_3$. Spin-glass or superparamganetic behaviors might be responsible for this hysteresis between ZFC and FC, AC susceptibility measurements or neutron scattering measurements constitutes future work to unveil the detailed mechanism.

Using the Curie-Weiss law $\chi = C/(T - \Theta)$ to fit the $1/\chi$ data of Cr_2Se_3 in the temperature range of 100 – 300 K, we obtain effective magnetic moment μ_{eff} = 3.85 μ_B per Cr ion and Weiss constant Θ = –158.6 K, respectively. The latter agrees well with Θ = –180 K reported by Adachi et al.[42] and indicates strong antiferromagnetic interactions before the antiferromagnetic transition at Néel temperature T_N = 50 K. The effective magnetic moment μ_{eff} was calculated from the formula $\mu_{eff} = \sqrt{7.997C}$ μ_B with μ_B = Bohr magneton and C = Curie constant = $N_A\mu_{eff}^2/3k_B$, where N_A is Avogadro's number = 6.02×10^{23}, μ_{eff} = effective magnetic moment and k_B = Boltzmann constant = 1.38×10^{-23} J K^{-1}.[43] The calculated value of μ_{eff} = 3.85 μ_B is in good agreement with the spin-only value for Cr^{3+} (μ_{eff} = 3.87 μ_B, with total spin S = 3/2 and the Landé factor g =2) and 3.84 μ_B reported by Yuzuri.[44] Smaller value 2.6 μ_B in Cr_2Se_3 at 6.5 K was reported by Adachi *et al.*[41] Here we also found μ_{eff} = 4.08 μ_B and 3.63 μ_B for $Cr_{1.96}Se_3$ and $Cr_{2.08}Se_3$, respectively. Correspondingly, the mean spin quantum numbers S are 3.2/2 and 2.8/2, assuming the Landé factor g =2.

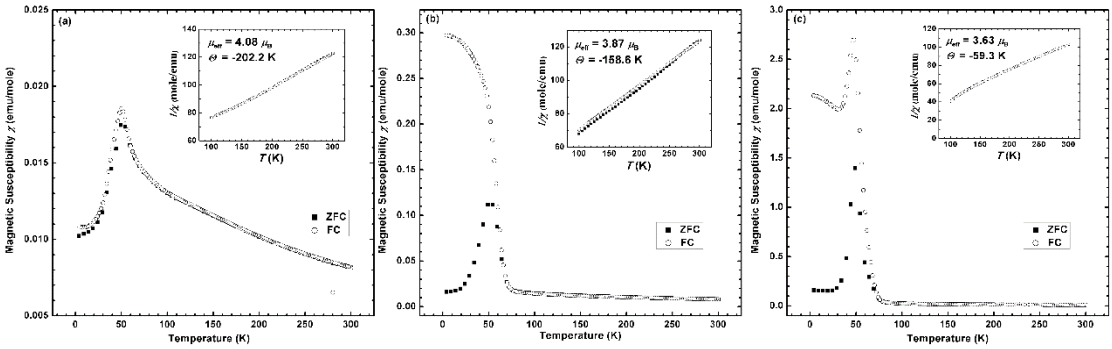

Figure 3. The temperature dependence of molar magnetic susceptibility χ, ZFC and FC curves of $Cr_{2+x}Se_3$ (x = –0.04, 0, 0.08). (a) x = –0.04; (b) x = 0; (c) x =0.08. The insets show the reciprocal susceptibility $1/\chi$ at 100 – 300 K.

The transport properties of five samples, $Cr_{2+x}Se_3$ (x = –0.04, –0.02, 0, 0.04, 0.08), are compared and listed in Table 1 and Table 2. The electrical conductivity data are presented in Figure 4. For samples with x = –0.04, –0.02, 0, each material exhibits a relatively high conductivity of similar magnitude, σ = ~ 550 $\Omega^{-1}cm^{-1}$ at 325 K, which decreases gradually to 350 $\Omega^{-1}cm^{-1}$ at 800 K with increasing temperature in every case. This temperature dependence is characteristic of degenerate semiconductors. The close σ values of samples with x = –0.04, –0.02, 0 could be attributed to their similar carrier concentrations (Table 1). As pointed out by Pisharody, adding additional chromium elements causes a decrease of the holes concentration because of the filling of the relevant valance band, resulting in a decreased electrical conductivity.[28] Although these predictions are not quite manifest in samples with x = –0.04, –0.02, 0 since $\sigma(x = -0.04) \approx \sigma(x = -0.02) \approx \sigma(x = 0)$, the electrical conductivity tends to decline when the Cr concentration reaches 0.04 (owing to a

remarkable decrease of carrier concentration by 70%, see Table 1) and drops further to ~ 200 $\Omega^{-1}cm^{-1}$ when x = 0.08 at 350 K. Hence experimentally we found $\sigma(x = -0.04) \approx \sigma(x = -0.02) \approx \sigma(x = 0) > \sigma(x = 0.04) > \sigma(x = 0.08)$.

Table 1. Density and electronic transport parameters for $Cr_{2+x}Se_3$ (x = –0.04, –0.02, 0, 0.04 and 0.08) estimated at room temperature.

Samples	**Density (g cm^{-3})**	**Hall Coefficient (cm^3/C)**	**Carrier Concentration (cm^{-3})**	**Hall Mobility (cm^2 V^{-1}s^{-1})**	**Effective Mass (m_0)**
$Cr_{1.96}Se_3$	5.66	6.25×10^{-2}	9.99×10^{19}	36.9	0.83
$Cr_{1.98}Se_3$	5.76	5.35×10^{-2}	1.17×10^{20}	31.5	0.95
Cr_2Se_3	5.52	5.52×10^{-2}	1.13×10^{20}	28.4	0.78
$Cr_{2.04}Se_3$	5.59	2.07×10^{-1}	3.02×10^{19}	124	0.51
$Cr_{2.08}Se_3$	5.46	-7.44×10^{-2}	-8.39×10^{19}	14.7	0.95

Table 2. Thermoelectric properties of $Cr_{2+x}Se_3$ (x = –0.04, –0.02, 0, 0.04, 0.08) at ~ 350 K \ 750 K.

Property	α (μVK^{-1})	σ (Ω^{-1}cm^{-1})	***P.F.*** (μW cm^{-1}K^{-2})	κ (Wm^{-1}K^{-1})	$ZT_{max}[T]$
$Cr_{1.96}Se_3$	90 \ 122	541 \ 361	4.36 \ 5.39	2.17 \ 2.61	0.16 [700 K]
$Cr_{1.98}Se_3$	90 \ 127	539 \ 362	4.40 \ 5.82	2.18 \ 2.63	0.18 [700 K]
Cr_2Se3	75 \ 112	479 \ 358	2.70 \ 4.47	2.13 \ 2.46	0.13 [700\750 K]
$Cr_{2.04}Se_3$	124 \ 152	499 \ 238	7.70 \ 5.52	2.16 \ 2.59	0.22 [600 K]
$Cr_{2.08}Se_3$	−154 \ −110	190 \ 215	4.54 \ 2.60	1.76 \ 2.40	0.13 [500 K]

It is worth mentioning that when x = 0.04 and x = 0.08, σ initially decreases slowly until the temperature reaches 600 K and 500 K and then begins to increase afterwards. The high temperature portion of the conductivity data was analysed exploiting the Arrhenius formula $\sigma = Aexp(-E_g/2k_BT)$, where A is a constant and E_g is the band gap. The results yielded E_g = 0.11 eV for x = 0.04 and E_g = 0.19 eV for x = 0.08, in accord with E_g = 0.156 eV previously reported by Chevreton *et al*.[45] These values are comparable to E_g = 0.15 eV for the commercialized Bi_2Te_3 and E_g = 0.2 eV for skutterudite $CoSb_3$.[46]

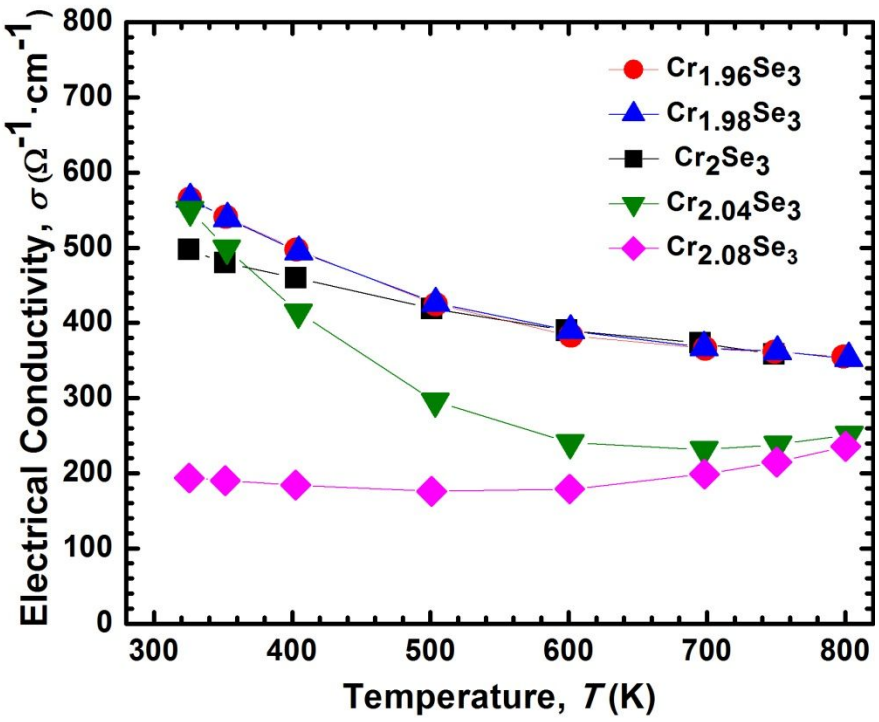

Figure 4. Electrical conductivity of $Cr_{2+x}Se_3$ with x = –0.04, –0.02, 0, 0.04 and 0.08. $\sigma(x = -0.04) \approx \sigma(x = -0.02) \approx \sigma(x = 0) > \sigma(x = 0.04) > \sigma(x = 0.08)$ at temperatures 400 – 800 K.

The electrical conductivity is proportional to the carrier concentration *via* $\sigma = ne\mu$, while the Seebeck coefficient typically follows the opposite trend, *i.e.* it increases with decreasing carrier concentration. As shown in Figure 5, our experiments confirmed the expectation that samples with larger σ values show smaller Seebeck coefficient: α (x = –0.04) ≈ α (x = – 0.02) ≈ α (x = 0) < α (x = – 0.04). Specifically, room temperature α values increase from α = +70 μV K^{-1} for samples with x = –0.04, –0.02, 0 to 120 μV K^{-1} for x = 0.04. In addition, the positive sign of α points towards *p*-type charge carriers, in agreement with the Hall measurement, as shown in Table 1. On the other hand, the sample with x = 0.08 actually exhibits a negative Seebeck

coefficient in the entire temperature range here. It indicates that the electrons begin to fill the conduction band and predominant carriers are electrons, which is consistent with the negative Hall coefficient taken on it (Table 1). Besides, the Seebeck coefficients of $x = 0.04$ and $x = 0.08$ increase at first with the increasing temperature, later on peak at around 600 K and 500 K, and then start to decrease, probably due to the onset of the intrinsic conduction. When both types of carriers (electrons and holes) are present, the Seebeck coefficient will be reduced since their relative contributions are subtractive.[47] This simple image has been qualitatively validated by their σ data. According to the relationship $E_g = 2e\alpha_{max}T_{max}$ (e = electron charge; α_{max} = maximum of α; T_{max} = the temperature at which α_{max} is achieved) proposed by Goldsmid and Sharp,[48] we estimate the band gap values: 0.22 eV for $Cr_{2.04}Se_3$ and 0.17 eV for $Cr_{2.08}Se_3$. In the latter case it is quite close the result calculated *via* Arrhenius equation. Incidentally, $E_g = 2e\alpha_{max}T_{max} = 0.21 \sim 0.23$ eV were also reported for $Cr_2Se_{3-3x}S_{3x}$($0 \leq x \leq 0.10$) solid solutions.[29] For comparison, a relatively larger $E_g(Cr_2Se_3) = 0.4$ eV was obtained from a UV/Visible/NIR spectrum (Figure S2), indicating more experimental and theoretical work are required for comprehensive understanding towards the electronic structure of these materials.

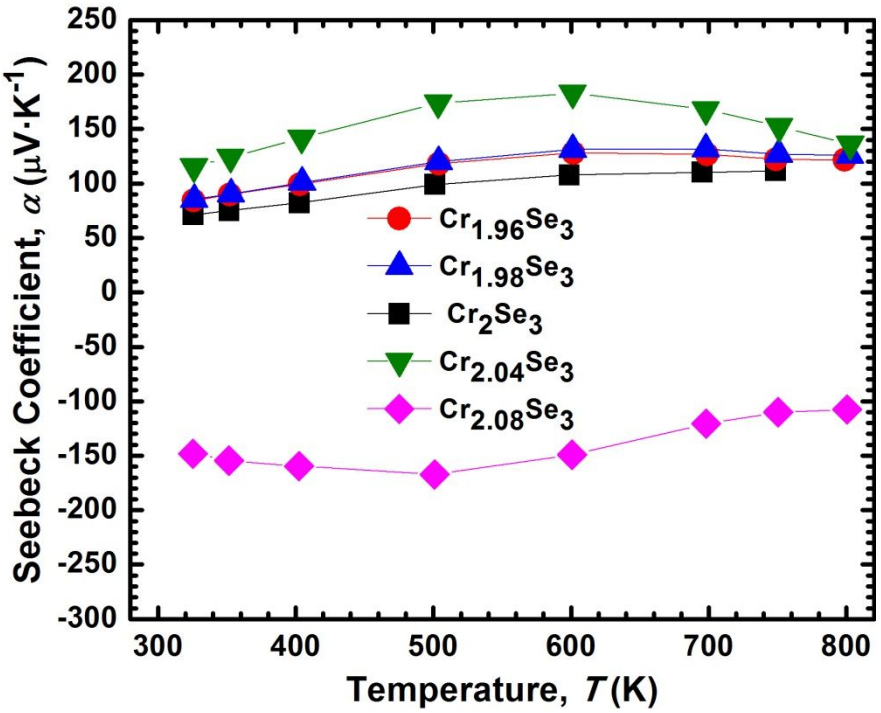

Figure 5. Seebeck coefficient of $Cr_{2+x}Se_3$(x = –0.04, –0.02, 0, 0.04, 0.08). Sample with x = 0.08 is an *n*-type material and the other cases are found *p*-type. α (x = –0.04) ≈ α (x = – 0.02) ≈ α (x = 0) < α (x = 0.04).

Figure 6 exhibits the temperature dependence of the thermal conductivity of $Cr_{2+x}Se_3$ (x = –0.04, –0.02, 0, 0.04, 0.08). The thermal conductivity, $\kappa = \kappa_E + \kappa_L$, is the sum of the electronic, κ_E, and lattice contributions, κ_L. The electronic part, $\kappa_E = L\sigma T$ (with L = Lorenz number) is proportional to the electrical conductivity and the temperature.[49] Here we found that the sample x = 0.08 that is accompanied by the lowest electrical conductivity shows the smallest thermal conductivity and κ(x = –0.04) ≈ κ(x = –0.02) > κ(x = 0) > κ(x = 0.04) > κ(x = 0.08) approximately in the temperature range 400 – 700 K. All samples have a κ in the range of 1.6 – 2.8 W $m^{-1}K^{-1}$. In addition, all of the κ values increase as the temperature increases from 300 K to 800

K, which is also observed in other metallic thermoelectric materials, *e.g.* Mo_3Sb_7 [50] and the ternary pseudo-hollandite $Ba_xCr_5Se_8$ ($0.5 < x < 0.55$).[51]

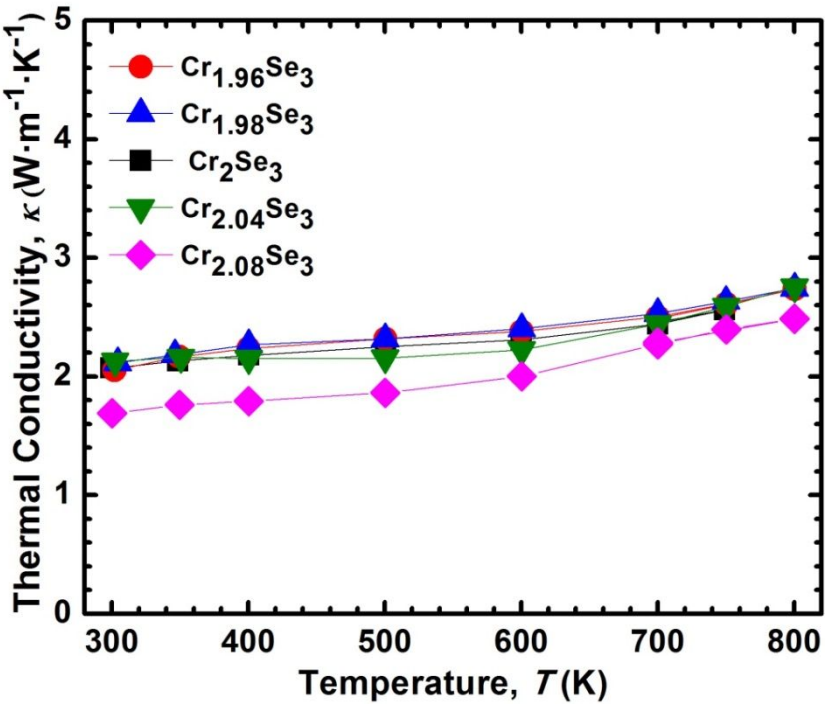

Figure 6. Thermal conductivity of $Cr_{2+x}Se_3$ with x = –0.04, –0.02, 0, 0.04 and 0.08. $\kappa(x = -0.04) \approx \kappa(x = -0.02) > \kappa(x = 0) > \kappa(x = 0.04) > \kappa(x = 0.08)$ at temperatures 400 – 700 K.

As illustrated in Figure 7, all samples have a κ_L in the range of 1.6 – 2.5 W $m^{-1}K^{-1}$, which means a high ratio κ_L to κ_E and hence the thermal conductivity mainly comes from the lattice part. The increase of the κ_L at higher temperatures should be attributed to the bipolar conduction. Here κ_L was obtained by subtracting the electronic part $\kappa_E = L\sigma T$ from the total thermal conductivity. In the Wiedemann–Franz law, the Lorenz number L is expressed by

$$L = \left(\frac{k_B}{e}\right)^2 \left\{\frac{3F_2(\eta)}{F_0(\eta)} - \left(\frac{2F_1(\eta)}{F_0(\eta)}\right)^2\right\}$$

And it could be solved from the experimentally measured Seebeck coefficient results *via*

$$|\alpha| = \frac{k_B}{e}\left\{\frac{2F_1(\eta)}{F_0(\eta)} - \eta\right\}$$

where $F_n(\eta)$ is the *n*-th order of Fermi integral. The calculated Lorenz numbers are in the range of 1.65 ~ 2.10 × 10^{-8} W ΩK^{-2}.

It is beneficial to compare the actual lattice thermal conductivity with the minimum lattice thermal conductivity κ_{min} since it will provide implications on to which extent the figure-of-merit could be optimized. Theoretically, κ_{min} is achieved under the assumption that the mean free path of the phonons is half of the wavelength of the phonons. Figure 7 also plotted the κ_{min} for Cr_2Se_3 calculated according to Cahill's formulation[52]

$$\kappa_{min} = \left(\frac{\pi}{6}\right)^{\frac{1}{3}} k_B \Delta^{-2} \sum_i v_i \left(\frac{T}{\Theta_i}\right)^2 \int_0^{\Theta_i/T} \frac{x^3 e^x}{(e^x - 1)^2} dx$$

where k_B = Boltzmann constant, Δ = the average volume per atom, $\Theta_i = v_i(\hbar/k_B)(6\pi^2 \Delta^{-3})^{1/3}$, and v_i = the sound velocity for the longitudinal and transverse modes. Here experimentally obtained longitudinal sound velocity (4098 m s^{-1}) and transverse sound velocity (2500 m s^{-1}) by Zhang et al. [29] were used for the calculation. Since κ_{min} is much lower than the experimental κ_L, there is tremendous scope for the reduction of the lattice thermal conductivity, for example, through solid solution formation, nanostructuring or the other promising techniques.[26]

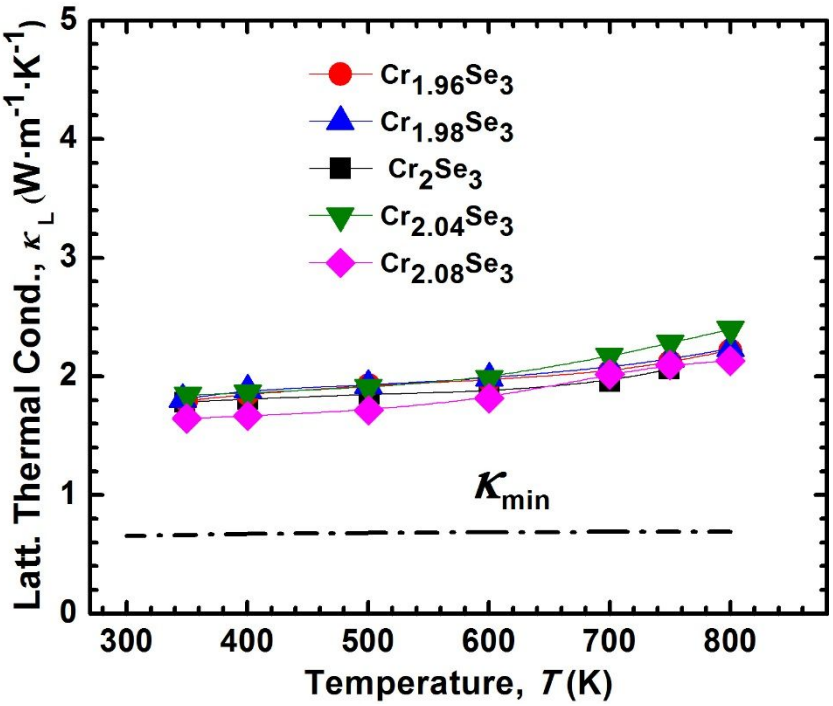

Figure 7. Lattice Thermal conductivity of $Cr_{2+x}Se_3$ with x = –0.04, –0.02, 0, 0.04 and 0.08. The minimum thermal conductivity κ_{min} (the dashed line) was also calculated and plotted.

Eventually, the figure-of-merit, *zTs* are calculated for all samples and shown in Figure 8. For samples with x = –0.04, –0.02 and 0, *zTs* first increase with increasing temperature and then decline slightly. Furthermore, the *zT*s of x = 0.04 and x = 0.08 peak at 600 K and 500 K, implying in both cases *zT*s are dominated by the Seebeck coefficient. Therefore, $Cr_{2.04}Se_3$ is identified as the most outstanding *p*-type material investigated here with a zT_{max} = 0.22 at 600 K. It is superior to the *p*–type polaron semiconductor $Fe_{0.9}Cr_{2.1}Se_4$, which possesses a zT_{max} = 0.15 at 525 K.[53] The *n*-type material $Cr_{2.08}Se_3$, with a Cr concentration corresponding to 2.08, shows a comparable zT_{max} = 0.13 at 500 K.

For further comprehensive and detailed understanding of the transport properties, preparation of single crystal samples could be interesting. On the other hand, nanostructuring and doping polycrystalline Cr_2Se_3 also appear attractive due to possibly lowered lattice thermal conductivity. In any cases, with excellent p-n control in a simple binary compound, Cr_2Se_3 exhibits high potential for intermediate temperature power generation.

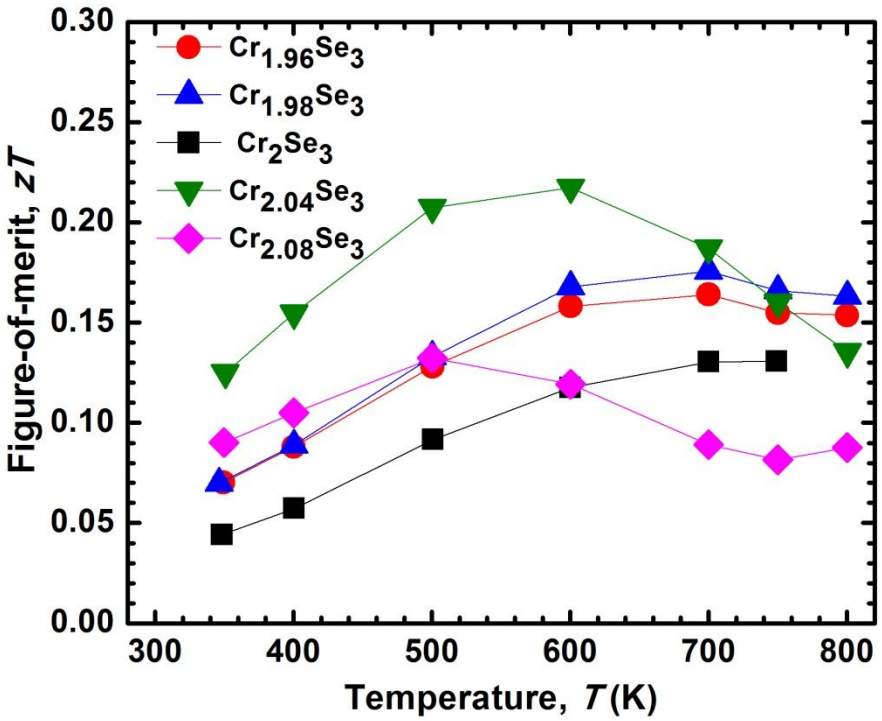

Figure 8. Figure-of-merit of $Cr_{2+x}Se_3$ with x = –0.04, –0.02, 0, 0.04 and 0.08. zT_{max} = 0.22 at 600 K for *p*-type $Cr_{2.04}Se_3$ and zT_{max} = 0.13 at 500 K for *n*-type $Cr_{2.08}Se_3$.

CONCLUSIONS

To conclude, we have successfully prepared a variety of modifications of Cr_2Se_3 by the solid state reaction and SPS method and characterized their magnetic, optical and thermoelectric performance. The results demonstrate that both *n*- and *p*- type chromium selenides could be prepared by facile composition tuning, making Cr_2Se_3 a potential candidate for intermediate temperature power generation. Seebeck coefficient and Hall measurements corroborate that $Cr_{2+x}Se_3$ is of *p*-type conduction when $-0.04 \leq x \leq 0.04$ and it turns out to be able to be converted to an *n*-type material when the Cr concentration is over 0.06 (Figure S1). By Curie-Weiss law, an effective magnetic moment μ_{eff} = 3.85 μ_B per Cr ion in Cr_2Se_3 is obtained, implying the principle contribution to the magnetic moments is from the spin. UV/Visible/NIR spectrum indicates an $E_g(Cr_2Se_3)$ = ~ 0.4 eV, which is higher than the $E_g(Cr_2Se_3)$ = 0.1 – 0.2 eV deduced from temperature dependence of electrical conductivity and Seebeck coefficient. The best *p*-type material here is $Cr_{2.04}Se_3$ with a zT_{max} = 0.22 at 600 K and its *n*-type counterpart, $Cr_{2.08}Se_3$, shows a comparatively lower zT_{max} = 0.13 at 500 K.

ACKNOWLEDGEMENTS

This work is supported by JST CREST Grant Number JPMJCR15Q6, Japan and JSPS KAKENHI Grant Numbers JP16H06441 and JP17H02749.

ASSOCIATED CONTENT

Supporting Information

Tauc plot, repeatability of thermoelectric properties and lattice parameters are available free of charge via the Internet at https://pubs.rsc.org.

AUTHOR INFORMATION

Corresponding author

Email: MORI.Takao@nims.go.jp

ORCID

Quansheng Guo 0000-0002-8936-4251

Jumpei Ueda 0000-0002-7013-9708

Setsuhisa Tanabe 0000-0002-7620-0119

Akinobu Miyoshi: 0000-0002-4557-8346

Kazuhiko Maeda: 0000-0001-7245-8318

Takao Mori: 0000-0003-2682-1846

Conflicts of interest

There are no conflicts to declare.

REFERENCES

1. D. M. Rowe, *Thermoelectrics Handbook: Macro to Nano*, CRC Press, Taylor & Francis Group, Boca Raton, FL, USA, 2006.
2. H. Akinaga, H. Fujita, M. Mizuguchi and T. Mori, *Sci. Technol. Adv. Mater.*, 2018, **19**, 543.
3. T. Mori and S. Priya, *MRS Bull.*, 2018, **43**, 176-180.

4. R. Tian, C. Wan, N. Hayashi, T. Aoai and K. Koumoto, *MRS Bull.*, 2018, **43**, 193-198.
5. I. Petsagkourakis, K. Tybrandt, X. Crispin, I. Ohkubo, N. Satoh and T. Mori, *Sci. Technol. Adv. Mater.*, 2018, **19**, 836-862.
6. G. S. Nolas, J. Sharp and H. J. Goldsmid, *Thermoelectrics: Basic Principles and new materials developments*, Springer, Berlin, 2001.
7. T. Mori, *Small*, 2017, **13**, 1702013.
8. G. J. Snyder and E. S. Toberer, *Nat. Mater.*, 2008, **7**, 105-114.
9. Y. Zheng, Q. Zhang, X. Su, H. Xie, S. Shu, T. Chen, G. Tan, Y. Yan, X. Tang and C. Uher, *Adv. Energy Mater.*, 2015, **5**, 1401391/1-11.
10. A. Pakdel, Q. Guo, V. Nicolosi and T. Mori, *J. Mater. Chem. A*, 2018, **6**, 21341-21349.
11. K. Biswas, J. He, I. D. Blum, C.-I. Wu, T. P. Hogan, D. N. Seidman, V. P. Dravid and M. G. Kanatzidis, *Nature*, 2012, **489**, 414-418.
12. E. S. Toberer, C. A. Cox, S. R. Brown, T. Ikeda, A. F. May, S. M. Kauzlarich and G. J. Snyder, *Adv. Funct. Mater.*, 2008, **18**, 2795-2800.
13. G. Rogl, A. Grytsiv, P. Rogl, N. Peranio, E. Bauer, M. Zehetbauer and O. Eibl, *Acta Mater.*, 2014, **63**, 30-43.
14. A. U. Khan, K. Kobayashi, D.-M. Tang, Y. Yamauchi, K. Hasegawa, M. Mitome, Y. Xue, B. Jiang, K. Tsuchiya and D. Golberg, *Nano Energy*, 2017, **31**, 152-159.
15. N. Farahi, S. Prabhudev, G. A. Botton, J. R. Salvador and H. Kleinke, *ACS Appl. Mater. Interfaces*, 2016, **8**, 34431-34437.
16. W. Liu, X. Tan, K. Yin, H. Liu, X. Tang, J. Shi, Q. Zhang and C. Uher, *Phys. Rev. Lett.*, 2012, **108**, 166601/1-5.
17. H. Tamaki, H. K. Sato and T. Kanno, *Adv. Mater.*, 2016, **28**, 10182-10187.
18. A. Maignan, Y. Bréard, E. Guilmeau and F. Gascoin, *J. Appl. Phys.*, 2012, **112**, 013716/1-5.
19. A. Maignan, E. Guilmeau, F. Gascoin, Y. Bréard and V. Hardy, *Sci. Technol. Adv. Mater.*, 2012, **13**, 053003/1-9.

20. N. Tsujii and T. Mori, *Appl. Phys. Express*, 2013, **6**, 043001/1-4.
21. R. Ang, A. U. Khan, N. Tsujii, K. Takai, R. Nakamura and T. Mori, *Angew. Chem. Int. Ed.*, 2015, **54**, 12909-12913.
22. H. Takaki, K. Kobayashi, M. Shimono, N. Kobayashi, K. Hirose, N. Tsujii and T. Mori, *Mater. Today Phys.*, 2017, **3**, 85-92.
23. A. U. Khan, R. A. R. A. Orabi, A. Pakdel, J.-B. Vaney, B. Fontaine, R. Gautier, J.-F. Halet, S. Mitani and T. Mori, *Chem. Mater.*, 2017, **29**, 2988-2996.
24. Q. Guo, J.-B. Vaney, R. Virtudazo, R. Minami, Y. Michiue, Y. Yamabe-Mitarai and T. Mori, *Inorg. Chem.*, 2018, **57**, 5258-5266.
25. F. Wehmeier, E. Keve and S. Abrahams, *Inorg. Chem.*, 1970, **9**, 2125-2131.
26. T. Zhang, X. Su, Y. Yan, W. Liu, T. Hu, C. Zhang, Z. Zhang and X. Tang, *ACS Appl. Mater. Interfaces*, 2018, **10**, 22389-22400.
27. T. Zhang, X. Su, J. Li, Z. Li, Y. Yan, W. Liu and X. Tang, *Inorg. Chem.*, 2018, **57**, 12125-12131.
28. K. Pisharody, *J.Solid State Chem.*, 1979, **30**, 149-156.
29. T. Zhang, X. Su, Y. Yan, W. Liu, Y. You, H. Xie, D. Yang, C. Uher and X. Tang, *J. Mater.Chem. C*, 2018, **6**, 836-846.
30. F. Ahmed, N. Tsujii and T. Mori, *J. Mater. Chem. A*, 2017, **5**, 7545-7554.
31. S. Acharya, S. Anwar, T. Mori and A. Soni, *J. Mater.Chem. C*, 2018, **6**, 6489-6493.
32. F. Ahmed, N. Tsujii and T. Mori, *J. Materiomics*, 2018, **4**, 221-227.
33. N. Tsujii, A. Nishide, J. Hayakawa and T. Mori, *Sci. Adv.*, 2019, **5**, eaat5935.
34. P. Qiu, Y. Qin, Q. Zhang, R. Li, J. Yang, Q. Song, Y. Tang, S. Bai, X. Shi and L. Chen, *Adv. Sci.*, 2017, **5**, 1700727/1- 8.
35. R. Sahara, T. Mori, S. Maruyama, Y. Miyazaki, K. Hayashi and T. Kajitani, *Sci. Technol. Adv. Mater.*, 2014, **15**, 035012/1-8.
36. O. Sologub, L. Salamakha, B. Stöger, Y. Michiue and T. Mori, *Acta Mater.*, 2017, **122**, 378-385.

37. J. Tauc, R. Grigorovici and A. Vancu, *Phys. Status Solidi B*, 1966, **15**, 627-637.
38. K. Sato, Y. Aman, M. Hirai and M. Fujisawa, *J. Phys. Soc. Jpn.*, 1990, **59**, 435-438.
39. A. C. Larson and R. B. Von Dreele, *General Structure Analysis System*, Los Alamos National Laboratory, Los Alamos, NM 87545, 2004.
40. B. H. Toby, *J. Appl. Crystallogr.*, 2001, **34**, 210-213.
41. Y. Adachi, M. Ohashi, T. Kaneko, M. Yuzuri, Y. Yamaguchi, S. Funahashi and Y. Morii, *J. Phys. Soc. Jpn.*, 1994, **63**, 1548-1559.
42. Y. Adachi, M. Yuzuri, T. Kaneko, S. Abe and H. Yoshida, *J. Phys. Soc. Jpn.*, 1994, **63**, 369-370.
43. R. L. Carlin, *Magnetochemistry*, Springer, New York, NY, USA, 1986.
44. M. Yuzuri, *J. Phys. Soc. Jpn.*, 1973, **35**, 1252.
45. M. Chevreton, M. Murat, C. Eyraud and E. F. Bertaut, *Journal de Physique*, 1963, **24**, 443-446.
46. X. Shi, L. Chen and C. Uher, *Int. Mater. Rev.*, 2016, **61**, 379-415.
47. C. Wood, *Rep. Prog. Phys.*, 1988, **51**, 459-539.
48. H. J. Goldsmid and J. W. Sharp, *J. Electr. Mater.*, 1999, **28**, 869-872.
49. R. Franz and G. Wiedemann, *Ann. Phys.*, 1853, **165**, 497-531.
50. C. Candolfi, B. Lenoir, A. Dauscher, E. Guilmeau, J. Hejtmánek, J. Tobola, B. Wiendlocha and S. Kaprzyk, *Phys. Rev. B*, 2009, **79**, 035114/1-6.
51. R. Lefèvre, D. Berthebaud, S. Bux, S. Hébert and F. Gascoin, *Dalton Trans.*, 2016, **45**, 12119-12126.
52. D. G. Cahill, S. K. Watson and R. O. Pohl, *Phys. Rev. B*, 1992, **46**, 6131-6140.
53. G. J. Snyder, T. Caillat and J.-P. Fleurial, *Phys. Rev. B*, 2000, **62**, 10185/1-9.

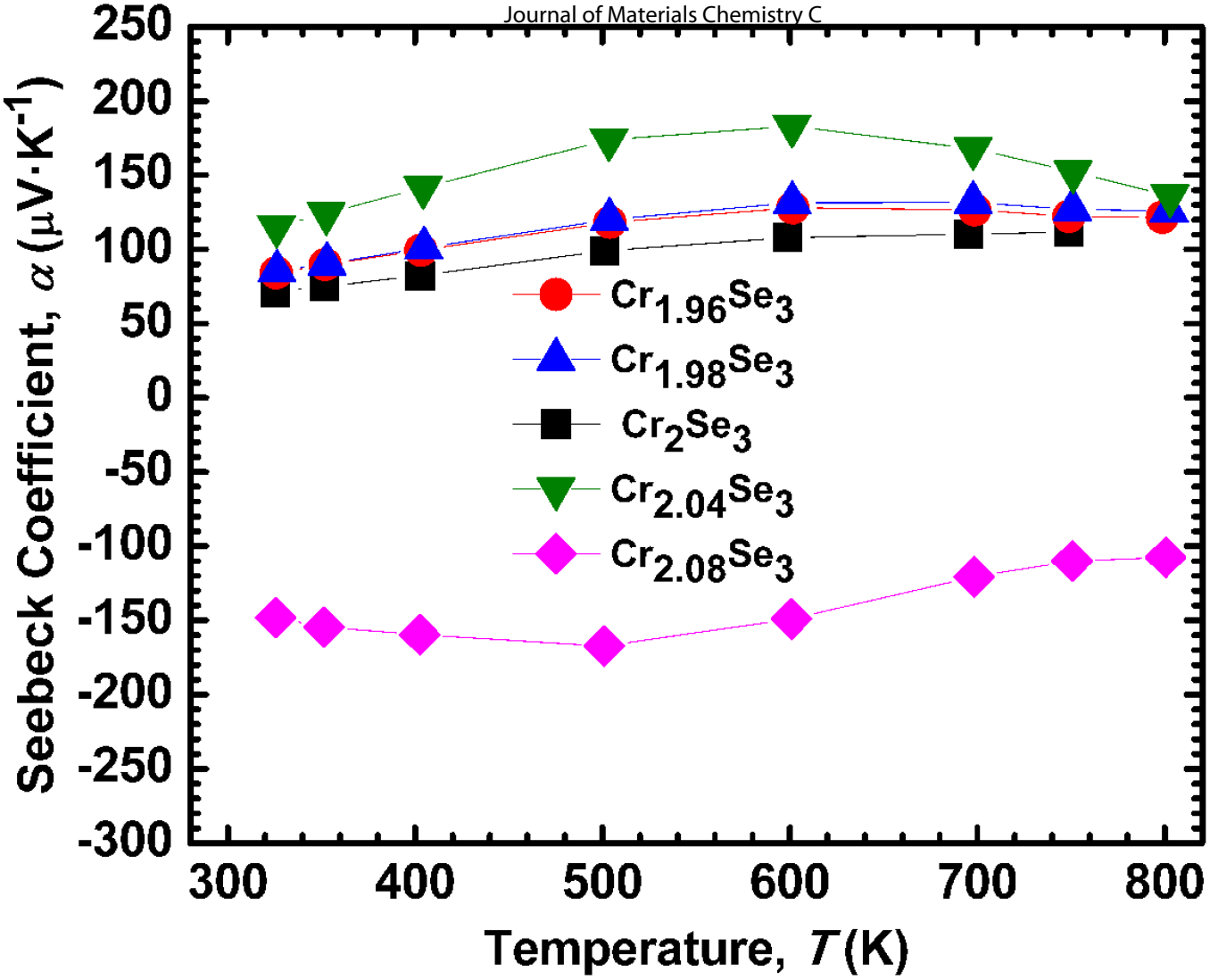

Both *n*- and *p*- type binary $Cr_{2+x}Se_3$ were prepared by composition tuning, aiming for thermoelectric applications near room temperature.